Available online at www.sciencedirect.com

ScienceDirect

IFAC PapersOnline CONFERENCE PAPER ARCHIVE

IFAC PapersOnLine 52-12 (2019) 316–321

Automatic Three-Point Landing of a UAV with H_∞-Control in $\mathcal{D}$-Implementation

Nicolas Sedlmair * **Julian Theis** * **Frank Thielecke** *

* *Institute of Aircraft Systems Engineering, Hamburg University of Technology, Hamburg, Germany. (e-mail: {nicolas.sedlmair, julian.theis, frank.thielecke}@tuhh.de).*

Abstract: A multivariable flight control law for automatic landing of an unmanned aircraft with tailwheel gear configuration is developed in this paper. The control law is obtained using H_∞-synthesis and implemented in a differential form to facilitate bumpless transfer, i.e. correct initialization when switching control laws, and anti-windup compensation. The controller is evaluated using a validated high-fidelity model of the aircraft and Monte-Carlo simulations.

Keywords: flight control, robust control applications, multivariable control systems

1. INTRODUCTION

The objective of the control law developed in this paper is to allow safe automatic landing of the 25 kg unmanned low-cost testing research aircraft (ULTRA) Extra, depicted in Fig. 1. The ULTRA-Extra is an unmanned replica of the aerobatic aircraft Extra 330 ML with a scale of 1:2.5 and has a tailwheel configuration. Several approaches for the automatic landing problem are discussed in the literature, e. g., Lambregts and Creedon (1980), Niewoehner and Kaminer (1996), Looye and Joos (2006), de Bruin and Jones (2016), Kügler and Holzapfel (2017), Navarro-Tapia et al. (2017), and Theis et al. (2018). However, all these designs consider aircraft in tricycle gear configuration where the acceptable pitch attitude at touchdown is large. The only requirements are that the main landing gear (MLG) touches ground first and that tailstrike is avoided, cf. Niewoehner and Kaminer (1996). In tailwheel (or conventional gear) configuration, the acceptable variation in pitch attiude is much smaller. The MLG is located forward of the aircraft's center of gravity such that bouncing can occur if the MLG touches down first. Similarly, touching down tailwheel first with a large pitch angle can lead to a fast impact of the MLG and cause damage. Thus, ideally all three wheels touch down simultaneously. Further, the sink rate at touchdown needs to be as low as possible to reduce impact forces. Some controllers for automatic landing directly address this target by tracking a sink rate command, e. g., Lambregts and Creedon (1980), Navarro-Tapia et al. (2017), and Theis et al. (2018). Others track a desired pitch attitude and indirectly reduce sink rate, e. g. Looye and Joos (2006). Yet others track a given height trajectory (e. g. Lambregts and Creedon (1980), Niewoehner and Kaminer (1996)) or switch between sink rate and attitude control (Kügler and Holzapfel (2017)). Lambregts (1982, 1983) highlights the importance of controlling both sinkrate and airspeed and proposes multivariable control with a combination of elevator and thrust. Niewoehner and Kaminer (1996) make use of the fast engine dynamics of the F-14 fighter to simultaneously track glideslope and angle-of-attack. Other multivariable control approaches make use of extra effectors such as spoilers (Kaminer and Khargonekar (1990), Niewoehner and Kaminer (1996)) or flaps (de Bruin and Jones (2016)) for direct lift control (DLC). These effectors provide additional authority to control vertical acceleration with a much lower effect on pitch attitude compared to elevators.

Fig. 1. Flight test aircraft ULTRA-Extra.

To meet the challenge of touching down with all three wheels simultaneously, this paper proposes to track both sink rate and pitch angle using a multivariable H_∞-control law for the flare maneuver. As this control law is active only during the final phase of the landing, a smooth transition into the control law is necessary. This implies proper initialization, i. e., the control signals need to be continuous and switching should not excite the controller dynamics. Further, integrator windup needs to be avoided, which is not trivial for general multivariable controllers, see e. g. Mulder et al. (2001); Turner and Postlethwaite (2004); Sofrony et al. (2007); Tarbouriech and Turner (2009). The $\mathcal{D}$-implementation, originally developed by Kaminer et al. (1995) addresses these issues. It implements controllers in a "differential" form, i. e., such that the derivative $\dot{u}$ instead of the control signal u is calculated. Such implementations are also referred to as velocity or incremental algorithms and have their roots in motor control, see e. g. Åström and Hägglund (2006). However, the $\mathcal{D}$-implementation proposed in Kaminer et al. (1995) can-

10.1016/j.ifacol.2019.11.262

not be directly applied to H_∞-controllers, as they generally do not exhibit the necessary structure. Thus, a slightly different formulation is developed in this paper which recovers the original result and is immediately applicable to H_∞-controllers. The paper starts with a short review of H_∞-control and the concept of a $\mathcal{D}$-implementation in Sec. 2. Section 3 derives the expression for the $\mathcal{D}$-implementation of H_∞-controllers. The control design is described in Sec. 4 and detailed nonlinear simulation results are finally presented in Sec. 5.

2. PRELIMINARIES

This section briefly reviews some fundamentals of H_∞-control and revisits the concept of a $\mathcal{D}$-implementation.

2.1 Mixed Sensitivity H_∞-Control

Consider a standard unity feedback control loop with plant P and controller K. Throughout this paper, the plant output is denoted $y = \left[\begin{smallmatrix} y_1 \\ y_2 \end{smallmatrix}\right]$, where y_1 are (integral-) controlled outputs and y_2 are additional feedback signals. Consequently, the control error is $e = \left[\begin{smallmatrix} y_{\mathrm{ref}} - y_1 \\ -y_2 \end{smallmatrix}\right]$, where y_{ref} is a reference. The control signal is denoted u. In mixed sensitivity control, performance is characterized in terms of the H_∞-norm of a weighted combination of closed-loop transfer functions. The fundamental closed-loop transfer functions are called the sensitivity $S = (I + PK)^{-1}$, control sensitivity KS, load disturbance sensitivity SP, and complementary sensitivity $T := I - S$, cf. Skogestad and Postlethwaite (2005). The control problem is posed as the optimization problem

$$\min_K \left\| \begin{bmatrix} W_e V_e^{-1} & 0 \\ 0 & W_u V_u^{-1} \end{bmatrix} \begin{bmatrix} S & SP \\ KS & KSP \end{bmatrix} \begin{bmatrix} V_e & 0 \\ 0 & V_d \end{bmatrix} \right\|_\infty . \tag{1}$$

A controller K with state space representation

$$\dot{x} = A_\infty\, x + B_\infty\, e \tag{2a}$$
$$u = C_\infty\, x \tag{2b}$$

can be obtained by iteratively solving two bounded-real type algebraic Riccati equations, see e. g. (Zhou et al., 1995, Theorem 16.4).

Desired shapes for the frequency responses of the sensitivity functions are imposed through frequency-dependent shaping filters W_e and W_u. A high gain in W_e dictates a sensitivity reduction, resulting in tracking and disturbance rejection capabilities. Conversely, a high gain in W_u dictates a reduction in control effort. Integral control with a specified bandwidth ω_b is usually realized my means of a stable filter $W_e = \frac{\omega_b}{\epsilon + s}$ with $\epsilon \ll 1$. This approximation is a more or less technical consequence of the requirement that the generalized closed-loop needs to be stable and the fact that W_e, being outside the actual loop, is not stabilizable by any choice of K, cf. (Zhou et al., 1995, Sec.17.4). Static weights V_e, V_u, and V_d are used as tuning knobs. They can be assigned the intuitive interpretation of maximum allowable errors (V_e), maximum allowable inputs (V_u), and maximum expected disturbances (V_d) which makes initial guesses particularly easy, see Theis (2018) for details about this parameterization. A signal interpretation of the generalized closed-loop interconnection in Eq. (1) is shown in Fig. 2 using fictitious inputs w_1, w_2 and outputs z_1, z_2 to represent loop break points.

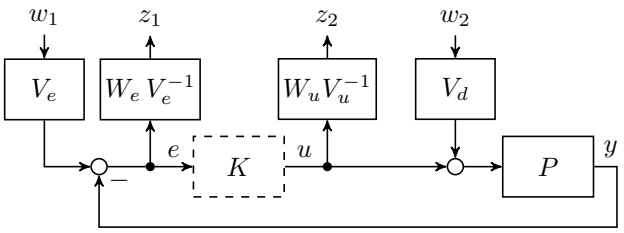

Fig. 2. Mixed sensitivity generalized plant interconnection.

2.2 $\mathcal{D}$-Implementation

The original $\mathcal{D}$-implementation, introduced by Kaminer et al. (1995), was developed as a means to circumvent excitation of so-called hidden couplings in gain-scheduled controllers, cf. also Nichols et al. (1993); Shamma and Cloutier (1993). It requires a controller with state space representation

$$\begin{bmatrix} \dot{x}_1 \\ \dot{x}_2 \end{bmatrix} = \begin{bmatrix} 0 & 0 \\ A_{21} & A_{22} \end{bmatrix} \begin{bmatrix} x_1 \\ x_2 \end{bmatrix} + \begin{bmatrix} I & 0 \\ 0 & B_{22} \end{bmatrix} \begin{bmatrix} y_{\mathrm{ref}} - y_1 \\ -y_2 \end{bmatrix} \tag{3a}$$

$$u = [C_1\ C_2] \begin{bmatrix} x_1 \\ x_2 \end{bmatrix} + [D_1\ D_2] \begin{bmatrix} y_{\mathrm{ref}} - y_1 \\ -y_2 \end{bmatrix} . \tag{3b}$$

The controller (3) is then implementated as

$$\begin{bmatrix} \dot{\xi}_1 \\ \dot{\xi}_2 \end{bmatrix} = \begin{bmatrix} 0 & C_2 \\ 0 & A_{22} \end{bmatrix} \begin{bmatrix} \xi_1 \\ \xi_2 \end{bmatrix} + \begin{bmatrix} C_1 & D_2 \\ A_{21} & B_{22} \end{bmatrix} \begin{bmatrix} y_{\mathrm{ref}} - y_1 \\ -\dot{y}_2 \end{bmatrix} \tag{4a}$$

$$u = [I\ 0] \begin{bmatrix} \xi_1 \\ \xi_2 \end{bmatrix} + [D_1\ 0] \begin{bmatrix} y_{\mathrm{ref}} - y_1 \\ -\dot{y}_2 \end{bmatrix} . \tag{4b}$$

Equation (4) essentially is a realization of $\frac{1}{s}\, K\, s$. Note that even though $\dot{y}_2$ appears explicitly, the input-output map $\left[\begin{smallmatrix} y_{\mathrm{ref}} - y_1 \\ -y_2 \end{smallmatrix}\right] \to u$ of Eq. (3) and (4) are identical. The $\mathcal{D}$-implementation thus only affects the internal representation of the controller state and enforces an integrator at the output side, cf. Lawrence (2001). A closed-loop equilibrium is attained for $y_1 - y_{\mathrm{ref}} = 0$, $y_2 = \bar{y}_2 = \text{const.}$, and $u = \bar{u} = \text{const.}$ The corresponding steady state of a $\mathcal{D}$-implemented controller is $\bar{\xi}_1 = \bar{u}$, $\bar{\xi}_2 = 0$. It is hence easy to initialize the controller with a desired output and the "correct" state when switching between different control laws, i. e., bumpless transfer can be achieved. This property becomes particularly apparent when a PI controller is considered, see Rugh and Shamma (2000); Åström and Hägglund (2006). The $\mathcal{D}$-implementation in this case is a PD controller in series with an integrator, such that the integrator state equals the controller output at all times and no other controller states exist. Another advantage of such an implementation is that standard anti-windup compensation schemes such as backcalculation and integrator clamping can be applied, even for multivariable controllers, see e. g. Osterhuber et al. (2004).

3. $\mathcal{D}$-IMPLEMENTATION OF H_∞-CONTROLLERS

Generally, H_∞-controllers as obtained in Eq. (2) do not satisfy the structure of Eq. (3) required for the original $\mathcal{D}$-implementation. Mehendale and Grigoriadis (2004, 2006) propose to implement general state space controllers (A, B, C, D) as

$$\dot{\xi} = A\, \xi + B\, \tfrac{\mathrm{d}}{\mathrm{d}t} e \tag{5a}$$
$$\dot{v} = C\, \xi + D\, \tfrac{\mathrm{d}}{\mathrm{d}t} e \tag{5b}$$
$$u = v. \tag{5c}$$

Unfortunately, this approach is only equivalent to the original formulation in the absence of tracked outputs y_1, as verified by inserting Eq. (3) into Eq. (5) and comparing the result with Eq. (4). Otherwise, uncontrollable modes may arise. Specifically, constant errors don't necessarily excite the controller at all and tracking cannot be guaranteed, even if the controller contains integral action.

This section introduces an expression for the $\mathcal{D}$-implementation which can directly be applied to H_∞-controllers. As described in Sec. 2.1, H_∞-controllers usually approximate integral action by very slow, but stable poles. An eigenvector decomposition of the controller (2) can be performed to separate the state variables into two disjoint sets that represents the integral-like dynamics x_1 (with state matrix $A_1 = \mathrm{diag}(-\epsilon_1, \ldots, -\epsilon_{n_{y1}}) \approx 0$) and the remaining faster dynamics x_2 (with state matrix A_2), see e. g. Kailath (1980). Replacing A_1 with 0 yields the modal state space realization

$$\begin{bmatrix}\dot{x}_1\\ \dot{x}_2\end{bmatrix} = \begin{bmatrix}0 & 0\\ 0 & A_2\end{bmatrix}\begin{bmatrix}x_1\\ x_2\end{bmatrix} + \begin{bmatrix}B_{11} & 0\\ B_{21} & B_{22}\end{bmatrix}\begin{bmatrix}y_{\mathrm{ref}}-y_1\\ -y_2\end{bmatrix} \tag{6a}$$

$$u = \begin{bmatrix}C_1 & C_2\end{bmatrix}\begin{bmatrix}x_1\\ x_2\end{bmatrix} \tag{6b}$$

of the controller K that now contains actual integrators. Due to the modal form, this modification does not affect higher frequency controller dynamics. Further, y_2 does not excite x_1, as integral control is performed only on y_1.

In order to derive the expression for the $\mathcal{D}$-implementation, linearity is exploited to decompose the controller K from Eq. (6) into a sum of two controllers, $u_1 = K_1\,(y_{\mathrm{ref}} - y_1)$ and $u_2 = K_2\,(-y_2)$. Next, differentiation before K and integration after K are added, which does not alter the input-output behavior as

$$\begin{aligned} u = K\begin{bmatrix}y_{\mathrm{ref}}-y_1\\ -y_2\end{bmatrix} &= \frac{1}{s}\,\left(K_1\,s\,(y_{\mathrm{ref}}-y_1) - K_2\,s\,y_2\right)\\ &= \frac{1}{s}\,\left(s\,K_1(y_{\mathrm{ref}}-y_1) - K_2\,\dot{y}_2\right). \end{aligned} \tag{7}$$

Note that the differentiation is carried out only on the measurements y_2. For y_1, the fact that K_1 contains explicit integrators is used to derive a state space realization for $\dot{u}_1 = s\,K_1\,(y_{\mathrm{ref}}-y_1)$. Differentiating the output of the state space representation (cf. Silverman (1969)) of K_1 yields

$$\begin{aligned}\dot{\zeta}_1 &= A_2\,\zeta_1 + B_{21}\,(y_{\mathrm{ref}}-y_1)\\ \dot{u}_1 &= C_2A_2\,\zeta_1 + (C_1B_{11}+C_2B_{21})\,(y_{\mathrm{ref}}-y_1).\end{aligned}$$

Hence, a complete state space realization for Eq. (7) is

$$\begin{bmatrix}\dot{\zeta}_0\\ \dot{\zeta}_1\\ \dot{\zeta}_2\end{bmatrix} = \begin{bmatrix}0 & C_2A_2 & C_2\\ 0 & A_2 & 0\\ 0 & 0 & A_2\end{bmatrix}\begin{bmatrix}\zeta_0\\ \zeta_1\\ \zeta_2\end{bmatrix} + \begin{bmatrix}C_1B_{11}+C_2B_{21} & 0\\ B_{21} & 0\\ 0 & B_{22}\end{bmatrix}\begin{bmatrix}y_{\mathrm{ref}}-y_1\\ -\dot{y}_2\end{bmatrix}$$

$$u = \begin{bmatrix}I & 0 & 0\end{bmatrix}\zeta,$$

where ζ_0 represents the integrator states, ζ_1 are the states of $s\,K_1$ and ζ_2 are the states of K_2. Performing a state space transformation $\begin{bmatrix}\xi_1\\ \zeta_1\\ \xi_2\end{bmatrix} = \begin{bmatrix}I & 0 & 0\\ 0 & I & 0\\ 0 & A_2 & I\end{bmatrix}\begin{bmatrix}\zeta_0\\ \zeta_1\\ \zeta_2\end{bmatrix}$ further renders ζ_1 unobservable and results in the $\mathcal{D}$-implementation

$$\begin{bmatrix}\dot{\xi}_1\\ \dot{\xi}_2\end{bmatrix} = \begin{bmatrix}0 & C_2\\ 0 & A_2\end{bmatrix}\begin{bmatrix}\xi_1\\ \xi_2\end{bmatrix} + \begin{bmatrix}C_1B_{11}+C_2B_{22} & 0\\ A_2B_{21} & B_{22}\end{bmatrix}\begin{bmatrix}y_{\mathrm{ref}}-y_1\\ -\dot{y}_2\end{bmatrix} \tag{8a}$$

$$u = \begin{bmatrix}I & 0\end{bmatrix}\begin{bmatrix}\xi_1\\ \xi_2\end{bmatrix} \tag{8b}$$

which has the exact same properties as the original $\mathcal{D}$-implementation (4). The state variables ξ_1 represent the integrator states and ξ_2 represents the differential controller dynamics, denoted $K_\mathcal{D}$ in Fig. 3.

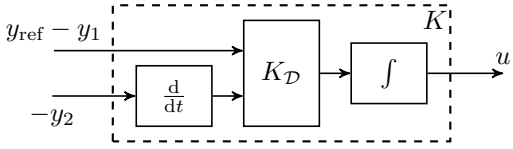

Fig. 3. $\mathcal{D}$-implementation of original controller K.

4. CONTROL DESIGN

The objective is to design a robust controller capable of landing the ULTRA-Extra aircraft in adverse environmental conditions. In lieu of an ILS-system, the automatic approach relies on a 3D spline-path-following algorithm developed and flight tested in Sedlmair et al. (2019). The control law tracks bank angle and sideslip angle for lateral-directional control such that a crabbed approach in crosswind is easily achieved. The following section focuses on longitudinal control design to meet the challenges of a three-point landing.

4.1 Problem Statement and Design Requirements

A multivariable flare controller that tracks both vertical speed and pitch attitude is designed. Elevator deflection, symmetrical aileron deflection, and thrust are the available control inputs. The ailerons, ranging across the whole wingspan, are included as additional DLC-like effectors. To ensure save landings, the design requirements for the controller are:

(1) The pitch angle at touchdown shall be 8°–12°.
(2) The vertical speed at touchdown shall not exceed 1.6 m/s (previous flight tests showed that no structural damage occurs below this limit).
(3) The deviation from the desired point of touchdown shall not exceed ±35 m (available window at test site to maintain enough runway length for rollout)
(4) The controller shall provide good performance in turbulent conditions including crosswind.
(5) The implementation shall ensure transient-free switching between control laws and include anti-windup compensation.

4.2 Synthesis Model

A linear time invariant (LTI) model is required for H_∞-controller synthesis. The nonlinear high-fidelity model of the ULTRA-Extra aircraft (see Sec. 5) is linearized for straight and level flight at 20 m/s airspeed. As shown in Sedlmair et al. (2019), longitudinal and lateral-directional motion can be decoupled. The longitudinal model contains short-period dynamics (natural frequency: 3.9 rad/s, damping ratio: 0.8) and phugoid dynamics (natural frequency: 0.5 rad/s, damping ratio: 0.2). Further, second-order actuator servo dynamics (natural frequency: 34 rad/s, damping ratio: 0.6), third-order engine dynamics (dominant time constant 0.14 s), and channel specific input time-delays are included.

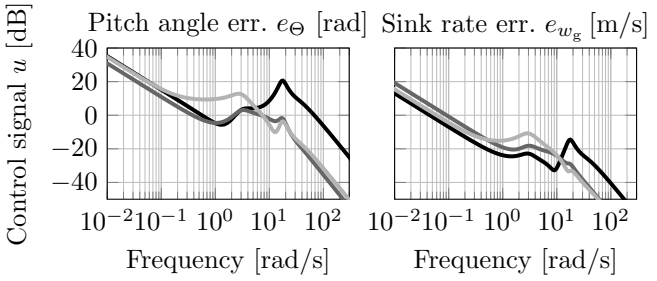

Fig. 4. Magnitude plot of H_∞-controller K to elevator (—), aileron (—), and thrust (—).

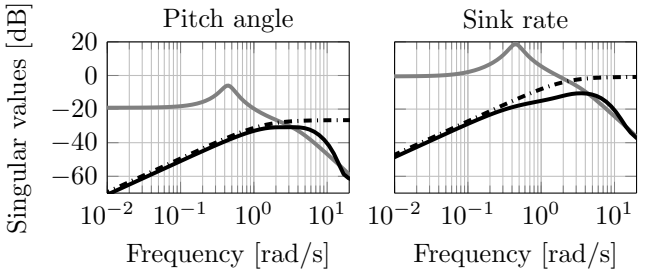

Fig. 5. Disturbance sensitivity SP: open-loop (—), closed-loop (—), inverse shaping filter (-·-).

4.3 Controller Design and Synthesis

The mixed sensitivity formulation of Sec. 2.1 is used for control design. To achieve tracking of step commands in pitch angle and vertical speed, the shaping filters W_e in Eq. (1) are chosen with integral-like behavior up to a bandwidth of 0.8 rad/s for pitch attitude and 1.2 rad/s for sink rate. Beyond this frequency, a gain of 0.5 is selected with the rationale to limit the peak sensitivity to a factor of two. The shaping filters W_u are specified with a slope of +20 dB per decade for frequencies above 20 rad/s for the elevators and the ailerons ($\approx 60\,\%$ of the actuator's bandwidth), and above 2 rad/s for the engine ($\approx 30\,\%$ of the engine's bandwidth). This ensures a roll-off in control effort and reduces noise sensitivity. The weight V_u is chosen based on physical interpretation: To retain sufficient roll authority, a maximum deflection of $V_{u,\delta_\mathrm{a}} = 8\,^\circ$ is selected for the DLC-like usage of the ailerons and $V_{u,\delta_\mathrm{e}} = 15\,^\circ$ for the elevators. For the engine, a weight $V_{u,\delta_\mathrm{thr}} = 0.5$ is used as a starting point. Tuning is done using the remaining scaling factors V_e and V_d. Choosing $V_{e,\Theta} = 0.8\,^\circ$, $V_{e,w_g} = 0.27\,\mathrm{m/s}$, $V_{d,\delta_\mathrm{e}} = 0.27\,^\circ$, $V_{d,\delta_\mathrm{a}} = 5.3\,^\circ$ and $V_{d,\delta_\mathrm{thr}} = 0.03\,^\circ$ led to a satisfactory controller. In the final design, $V_{u,\delta_\mathrm{thr}}$ was adjusted to 0.53.

The controller is synthesized using the `hinfsyn` function of Matlab. Its magnitude plot is shown in Fig. 4 for all inputs and outputs. Integral behavior at low frequencies and the desired roll-off at higher frequencies are evident. Figure 5 shows the singular value plots of the disturbance sensitivities for both tracked outputs. The improvements are clearly visible by comparing open-loop and closed-loop magnitude. Disturbance attenuation is achieved up to a bandwidth of 3 rad/s. Little but well-behaved amplification exists between 3 rad/s and 10 rad/s. The controller is $\mathcal{D}$-implemented according to Eq. (8) and executed at 50 Hz. Anti-windup compensation is included using integrator-clamping at the controller output.

5. CONTROLLER EVALUATION

Controller performance is evaluated using a nonlinear high-fidelity simulation model of the ULTRA-Extra aircraft, cf. Sedlmair et al. (2019). The model comprises computations of forces and moments due to propulsion, the interaction between the landing gear and ground, and aerodynamics including ground effect and dynamic asymmetric stall characteristics. An extensive flight test campaign with a total of 148 identification maneuvers was performed in order to identify aerodynamic parameters for a gray-box model using the output error method of Jategaonkar (2006). The moment of inertia tensor and the spring stiffness of the carbon landing gear were determined through experiments. The electric propulsion system was modeled using data gathered in a wind tunnel campaign where the thrust and the moment at the support were measured for varying airspeed, angle of attack, angle of sideslip and throttle position. The dynamics of the control surface servos where identified and the model includes time delay and backlash. Measurement noise, transport delays and signal filtering are also included. Environmental effects are simulated using vertical wind shear and atmospheric turbulence according to MIL-F-8785C. Further, a detailed ground model of an unpaved uneven runway is included.

5.1 Simulation Results

The simulation is initialized with the aircraft approximately 60 m above ground while heading in runway direction with an airspeed $V_\mathrm{A} = 20\,\mathrm{m/s}$. The scenario is designed such that the desired flight path during final approach is approximately a line with slope $\gamma_0 \approx -6\,^\circ$. In the initial approach phase, the path-following algorithm is active. Aileron deflection (δ_a) is used to track the desired path in lateral-direction. Elevator deflection (δ_e) generates vertical acceleration to assure vertical path tracking. Thrust (δ_thr) is commanded by an autothrottle. In the presence of crosswind, sideslip angle control assures aerodynamically clean flight through rudder deflection. Once the aircraft is below a fixed altitude above ground ($H_0 = 18\,\mathrm{m}$), the flare maneuver is engaged. Longitudinal motion control is now switched to the H_∞-controller. This switching must occur bumpless, which is achieved through the $\mathcal{D}$-implementation. The lateral-directional motion remains to be controlled by the path-following algorithm. During the flare maneuver, sink rate reference is calculated in dependence on the altitude above ground according to Theis et al. (2018). The desired sink rate at touchdown is $w_\mathrm{g,TD} = 0.6\,\mathrm{m/s}$. The pitch angle command is calculated as a function of the current altitude above ground H as

$$\Theta_\mathrm{cmd} = \Theta_0 + \frac{\Theta_\mathrm{TD} - \Theta_0}{H_0 - H_\mathrm{offset}} \cdot (H_0 - H). \tag{9}$$

Here, Θ_0 and Θ_TD are the pitch angle at flare initiation and the desired angle at touchdown. The height offset $H_\mathrm{offset} > 0$ guarantees that the desired pitch angle at touchdown is commanded shortly before touchdown. The maximum command is $\Theta_\mathrm{cmd} = \Theta_\mathrm{TD}$. At $H = 1\,\mathrm{m}$, the decrab maneuver is initiated to align the landing gear with the runway direction using the angle-of-sideslip control loop. Bank angle control ensures horizontal touchdown, i. e., $\Phi_\mathrm{TD} = 0°$.

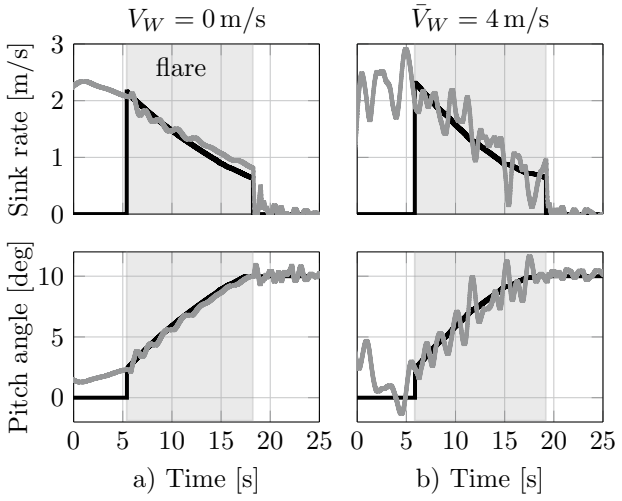

Fig. 6. Simulation results in still and turbulent air: command (—) and value (—).

Figure 6 shows simulation results for both still air and turbulent conditions. It is evident that the multivariable H_∞-controller shows excellent tracking performance in still air conditions. The pitch angle at touchdown is exactly $\Theta_{\mathrm{TD}} = 10\,^\circ$ and the sink rate is $w_{\mathrm{g,TD}} \approx 0.8\,\mathrm{m/s}$. The small error regarding sink rate is due to the ramp-type reference. The right plots in Fig. 6 show a landing where the aircraft is exposed to $90\,^\circ$ crosswind from the left. Mean wind speed is $\bar{V}_{\mathrm{W}} = 4\,\mathrm{m/s}$, which is about 20 % of the aircraft's airspeed. Turbulence and wind shear further complicate the situation. The H_∞-controller nevertheless shows very good performance in terms of turbulence attenuation and tracking. The pitch angle at touchdown is $\Theta_{\mathrm{TD}} \approx 9.6\,^\circ$ and the sink rate is $w_{\mathrm{g,TD}} \approx 0.9\,\mathrm{m/s}$. Figure 7 shows the control signals for the simulation in turbulent air. Higher control effort in elevator deflection and thrust are visible during flare. Regarding the ailerons, the results of the DLC-strategy are evident. During flare, an increased aileron activity is visible with deflections not being symmetrical to zero anymore. The requirement of bumpless switching between control laws is satisfied, as can be seen at flare initiation.

5.2 Monte-Carlo Evaluation

A Monte-Carlo evaluation with the nonlinear simulation model is performed to further investigate the performance of the H_∞-controller. To emulate varying environmental conditions, randomized parameters with uniform distributions are chosen for mean wind speed ($\bar{V}_W \in [0 \ldots 4]\,\mathrm{m/s}$) and mean wind direction ($\Delta\Psi_W = \pm 90\,^\circ$). The desired pitch angle and vertical speed at touchdown are $\Theta_{\mathrm{TD}} = 10\,^\circ$ and $w_{\mathrm{g,TD}} = 0.6\,\mathrm{m/s}$. As a benchmark, the baseline flight controller (BFC), as described in Sedlmair et al. (2019), is used. In contrast to the proposed H_∞-controller, the BFC tracks airspeed and sink rate during flare through separate single-loop controller cascades using throttle and elevator deflection, respectively. The sink rate reference is calculated in the same way as for the H_∞-controller. At flare initiation, airspeed reference is set to a fixed value of $V_A = 18\,\mathrm{m/s}$. Lateral-directional control as well as flare and decrab initiation heights are the same for both controllers.

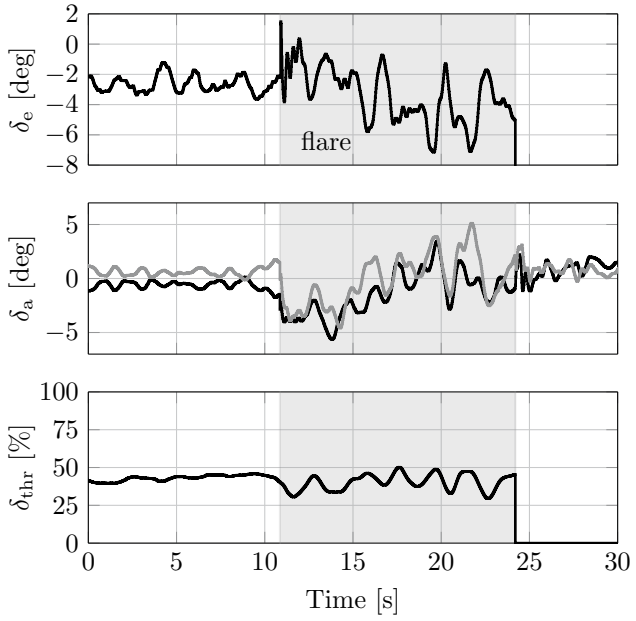

Fig. 7. Control signals during simulation in turbulent air.

Figure 8 shows the results of 6000 simulations for each controller. Figure 8a) depicts the vertical speed at touchdown. The H_∞-controller clearly reduces the probability of hard landings. The specified 1.6 m/s sink rate target is satisfied in 99.8 % of the simulated landings with the H_∞-controller compared to 96.4 % with the BFC. Vertical speed at touchdown is less than 1 m/s in $\approx$ 79 % of the simulations with the BFC, compared to $\approx$ 86 % with the H_∞-controller. Moreover, the highest vertical speed observed dropped from probably catastrophic 2.6 m/s (BFC) to 1.9 m/s (H_∞). The requirement is thus satisfied with an acceptable level of risk left.

Histograms regarding pitch angle at touchdown are shown in Fig. 8b). Again, significant improvements are visible. The probability of meeting the specified range of 8°–12° pitch angle at touchdown is 89.7 % for the BFC. Using the H_∞-controller, this probability is improved to 99.7 %. Moreover, the extreme values are reduced from $[\Theta_{\min}, \Theta_{\max}] = [3.4\,^\circ, 16.0\,^\circ]$ for the BFC to $[\Theta_{\min}, \Theta_{\max}] = [7.0\,^\circ, 12.8\,^\circ]$ for the H_∞-controller. That is, the requirement regarding pitch angle at touchdown is fulfilled. The risk is significantly reduced compared to the BFC. The deviation from the desired point of touchdown is depicted in Fig. 8c). A deviation of less than the required ± 35 m is achieved with a probability of 94.2 % for the BFC compared to 97.1 % for the H_∞-controller.

6. CONCLUSION

A multivariable flare control law is poposed to achieve three-point landing for a 25 kg UAV. The controller is designed using the H_∞ mixed sensitivity framework and simultaneously tracks pitch attitude and sink rate. To meet bumpless transfer and anti-windup compensation requirements, an expression for implementation of H_∞-controllers in differential form was introduced. A clear benefit of using the proposed controller over a conventional decoupled control approach was shown in various simulation trials.

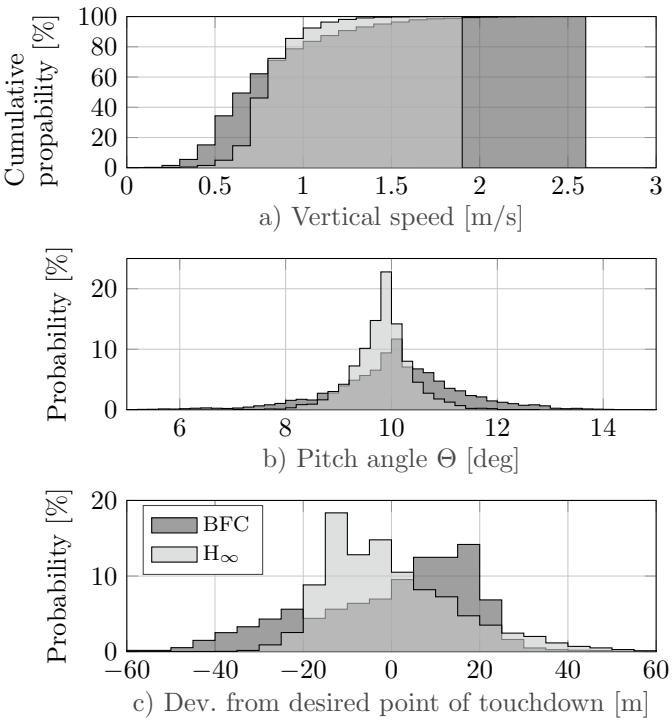

Fig. 8. Monte-Carlo evaluation in varying wind conditions.

REFERENCES

Åström, K. and Hägglund, T. (2006). *Advanced PID Control*. Instrumentation, Systems & Automation Society.

de Bruin, A. and Jones, T. (2016). Accurate autonomous landing of a fixed-wing unmanned aircraft under crosswind conditions. In *20th IFAC Symp. Automatic Control in Aerospace*.

Jategaonkar, R.V. (2006). *Flight Vehicle System Identification*. AIAA.

Kailath, T. (1980). *Linear Systems*. Prentice Hall, Englewood Cliffs, NJ.

Kaminer, I. and Khargonekar, P.P. (1990). Design of the flare control law for longitudinal autopilot using H_∞ synthesis. In *IEEE Conf. Decision and Control*, 2981–2986.

Kaminer, I., Pascoal, A.M., Khargonekar, P.P., and Coleman, E.E. (1995). A velocity algorithm for the implementation of gain-scheduled controllers. *Automatica*, 31(8), 1185–1191.

Kügler, M.E. and Holzapfel, F. (2017). Autoland for a novel UAV as a state-machine-based extension to a modular automatic flight guidance and control system. In *American Control Conf.*, 2231–2236.

Lambregts, A. (1982). Avoiding the pitfalls in automatic landing control system design. In *AIAA Guidance and Control Conf.*

Lambregts, A. and Creedon, J. (1980). Development and flight evaluation of automatic flare laws with improved touchdown dispersion. In *AIAA Guidance and Control Conf.* Paper 80-1757.

Lambregts, A. (1983). Vertical flight path and speed control autopilot design using total energy principles. In *AIAA Guidance and Control Conf.*

Lawrence, D.A. (2001). Gain scheduled controllers with guaranteed linear properties. In *American Control Conf.*, 4128–4133.

Looye, G. and Joos, H.D. (2006). Design of autoland controller functions with multiobjective optimization. *J. Guidance, Control, and Dynamics*, 29(2), 475–484.

Mehendale, C.S. and Grigoriadis, K.M. (2004). A new approach to LPV gain-scheduling design and implementation. In *IEEE Conf. Decision and Control*, 2942–2947.

Mehendale, C.S. and Grigoriadis, K.M. (2006). Performance of LPV gain-scheduled systems. In *American Control Conf.*, 2915–2920.

Mulder, E.F., Kothare, M.V., and Morari, M. (2001). Multivariable anti-windup controller synthesis using linear matrix inequalities. *Automatica*, 37, 1407–1416.

Navarro-Tapia, D., Simplicio, P., Iannelli, A., and Marcos, A. (2017). Robust flare control design using structured H_∞ synthesis: A civilian aircraft landing challenge. In *IFAC PapersOnLine*, volume 50, 2971–3976.

Nichols, R., Reichert, R., and Rugh, W. (1993). Gain scheduling for H_∞ controllers: A flight control example. *IEEE Trans. Control Systems Technology*, 1(2), 69–79.

Niewoehner, R.J. and Kaminer, I.I. (1996). Design of an autoland controller for an F-14 aircraft using H_∞ synthesis. *J. Guidance, Control, and Dynamics*, 19(3), 656–663.

Osterhuber, R., Hanel, M., and Hammon, R. (2004). Realization of the Eurofighter 2000 primary lateral/directional flight control laws with differential PI-algorithm. In *AIAA Guidance, Navigation, and Control Conf.*

Rugh, W.J. and Shamma, J.S. (2000). Research on gain scheduling. *Automatica*, 36, 1401–1425.

Sedlmair, N., Theis, J., and Thielecke, F. (2019). Design and experimental validation of UAV control laws – 3D spline-path-following and easy-handling remote control. In *5th CEAS Conf. Guidance, Navigation & Control*.

Shamma, J.S. and Cloutier, J.R. (1993). Gain-scheduled missile autopilot design using linear parameter varying transformations. *J. Guidance, Control, and Dynamics*, 16(2), 256–263.

Silverman, L.M. (1969). Inversion of multivariable linear systems. *IEEE Trans. Automat. Contr.*, 14(3), 270–276.

Skogestad, S. and Postlethwaite, I. (2005). *Multivariable Feedback Control*. Prentice Hall, Upper Saddle River, NJ, 2nd edition.

Sofrony, J., Turner, M.C., and Postlethwaite, I. (2007). Anti-windup synthesis using Riccati equations. *Int. J. Control*, 80(1), 112–128.

Tarbouriech, S. and Turner, M.C. (2009). Anti-windup design: an overview of some recent advances and open problems. *IET Control Theory & Appl.*, 3(1), 1–19.

Theis, J. (2018). *Robust and linear parameter-varying control of aeroservoelastic systems*. Ph.D. thesis, Hamburg University of Technology. URL `https://doi.org/10.15480/882.1635`.

Theis, J., Ossmann, D., Thielecke, F., and Pfifer, H. (2018). Robust autopilot design for landing a large civil aircraft in crosswind. *Control Engineering Practice*, 76, 54–64.

Turner, M.C. and Postlethwaite, I. (2004). A new perspective on static and low order anti-windup synthesis. *Int. J. Control*, 77(1), 27–44.

Zhou, K., Doyle, J.C., and Glover, K. (1995). *Robust and Optimal Control*. Prentice Hall, Upper Saddle River, NJ.